PAPER

Thermal induced NDC of electron swarms in N_2 and N_2-like gases: the role of temperature and collision operator approximations

View the article online for updates and enhancements.

IOP ebooks™

Bringing you innovative digital publishing with leading voices to create your essential collection of books in STEM research.

Start exploring the collection - download the first chapter of every title for free.

Thermal induced NDC of electron swarms in N$_2$ and N$_2$-like gases: the role of temperature and collision operator approximations

M J E Casey[1] , **D G Cocks**[1,5] , **G J Boyle**[1,6] , **M J Brunger**[2], **S Dujko**[3] , **J de Urquijo**[4] **and R D White**[1]

[1] College of Science and Engineering, James Cook University, Townsville QLD 4810, Australia
[2] College of Science and Engineering, Flinders University, GPO Box 2100, Adelaide, SA 5001, Australia
[3] Institute of Physics, University of Belgrade, Pregrevica 118, 11080 Belgrade, Serbia
[4] Instituto de Ciencias Físicas, Universidad Nacional Autónoma de México, 62251, Cuernavaca, Morelos, México

E-mail: Ronald.White@jcu.edu.au

CrossMark

Abstract

The role of temperature on the existence of negative differential conductivity (NDC) is investigated using Boltzmann equation calculations of electron swarms in gaseous nitrogen. This effect has been observed previously in both experimental results and calculations, with the important role of superelastic rotational collisional processes in this phenomenon being examined in this work. A simple analytic model cross-section set is employed to elucidate the role of de-excitation processes in NDC, with complementary physics identified in N$_2$. The criterion of Robson (1984 *Aust. J. Phys.* **37** 35) for predicting the occurrence of NDC using only knowledge of the collisional cross-sections is utilised for both the model system and N$_2$, and found to be in excellent agreement with our simulated appearance of NDC. Finally, we also report on the impact of anisotropy in the very low threshold scattering channels on the transport coefficients, examine the finite difference collision operator of Frost and Phelps (1962 *Phys. Rev.* **127** 1621) for the inelastic channel, in particular its neglect of recoil, and assess other assumptions utilised in existing Boltzmann equation solvers.

Keywords: negative differential conductivity, molecular nitrogen N$_2$, electron, multi-term Boltzmann equation

1. Introduction

As a swarm of electrons drift and diffuse through a background medium, driven out of equilibrium by an externally applied electric field, there can exist a region where the drift velocity of the electrons decreases with increasing electric field strength. This phenomenon, known as negative differential conductivity (NDC), has been comprehensively studied, both experimentally and theoretically [1, 2]. In both plasma and swarm physics NDC is present in gases used for

dosimetry and particle detectors [3–5], and has implications on the operating ranges of gas lasers with NDC-induced electric current oscillations in electron-beam-sustained discharge switches [6, 7]. For fundamental physics, NDC has played a role in evaluating complete and accurate scattering cross-section sets [8, 9]. Argon, for example, was considered to be a candidate for NDC in a pure gas, but this was later shown to be due to the presence of molecular impurities in the argon samples [10], and in gaseous mercury it has recently been shown that NDC occurs due to the presence of dimers [11]. Swarms of electrons can also induce NDC in liquids [12] and plasmas [13, 14], and NDC has been shown to be induced by positron swarms in argon [15]. In addition to NDC for positrons in argon, the same phenomenon has been

observed in water vapour [16], molecular hydrogen [17] and CF_4 [18]. As such, modelling systems to predict regions of NDC and the conditions of electron-induced NDC is of particular interest [1, 19].

In model systems, the work of Petrović *et al* [1] and Vrhovac and Petrović [20] detail different systems involving elastic, inelastic and ionisation cross-sections that, under various conditions, either enhance or eliminate the occurrence of an NDC region. Further to the electron and positron experimental studies, in real systems, the existence of NDC has been observed experimentally in gaseous systems of N_2 [21, 22], CH_4, CF_4 [23] and Hg [11], and predicted theoretically due to electron–electron interactions [14] in plasmas of Xe [24, 25], and Ar and Kr [24], to name but a few. NDC in gas mixtures also has an extensive history, observed in mixtures with helium, argon, N_2 and CH_4 [2, 13, 23, 26, 27]. In strongly attaching gases, NDC has also been shown to be induced through a combination of attachment heating and inelastic cooling [28].

Throughout this broad body of work, the sources of NDC have been discussed in detail by the various authors and a number of criteria have been proposed. Some of the conditions under which NDC can occur include the presence of inelastic collision channels, favoured particularly by a decreasing inelastic cross-section, the presence of a Ramsauer–Townsend minimum in the elastic momentum-transfer cross-section, or a rapidly increasing elastic momentum-transfer cross-section. However these are not necessary and sufficient conditions. The validity of these early criteria on the understanding of NDC was discussed in detail in Petrović *et al* [1] who address the analyses of Kleban and Davis [29, 30], Long and co-workers [10], and Lopantseva and co-workers [6], in particular, and in Vrhovac and Petrović [20] where consistency with the Shizgal [31] criterion is discussed. Of particular note are the simulations of Petrović *et al* [1] for N_2 that confirm that the presence of inelastic processes, other than rotational excitations, decreases the range of the NDC region, indicating that the rotational collisions are responsible for the presence of NDC, where the elastic cross-section is relatively isotropic. NDC in N_2 is of particular interest here, where a clear temperature dependence is observed. NDC is present in both experimental measurements [21, 32] and Boltzmann calculations [1, 33] at 77 K and 77.6 K, but absent at 293 K. This is explored further in this work, where the effect of temperature on the presence or absence of NDC is examined. The thermally induced NDC region in N_2 below room temperature is detailed. Here, the contribution of inelastic ground-state and excited-state collisional processes to the net energy transfer to and from the electron swarm are shown to be responsible for the extent of an NDC region.

The various criteria for the presence of NDC in these early works, as noted above, have been discussed in detail by the respective authors. Of particular interest here is the criterion proposed by Robson [19], where momentum-transfer theory was used to derive an expression based on the rate of change of the ratio of inelastic to elastic energy transfer with energy. This criterion allows prediction of NDC using only a knowledge of the collisional cross-sections, the accuracy of which is highlighted here using both a simple model system

and for N_2. The thermally-induced reduction and deactivation of NDC is explored further using Robson's criterion.

A model collisional system is used throughout this study to simplify discussions around NDC and its temperature dependence. This allows the relevant physics to be extracted with the use of simple analytical expressions, where no ambiguity in the functional form of the cross-sections exists. The model system is also used to verify both our solution method, and explicitly test the inclusion of temperature dependent isotropic and anisotropic inelastic collisions. These results can be used for benchmarking of future solution methods, with our present calculations and the independent Monte-Carlo method utilised here. The model system also facilitates further discussion around some of the assumptions sometimes involved in swarm modelling. The explicit effect of anisotropy in low-threshold inelastic processes is assessed, as well as the commonly employed two-term approximation [34], as is the neglect of superelastic collisions in higher-order collisional terms. Also assessed is the neglect of the recoil of the neutral particle during inelastic collisions in the Frost-Phelps [33] excitation collision operator, as utilised in many Boltzmann equation solutions. Truncation of the mass ratio expansion at zeroth order for inelastic collisions is compared with the exact collision description of Monte-Carlo simulations, for very low-energy threshold processes like rotational excitations, where the energy exchange is much closer to that for elastic collisions. For application of this discussion to real gases, these assumptions are also assessed for electron swarms in N_2. For the low energy regime of interest in this study, the discrete rotational collisions in N_2 are treated using the Frost-Phelps collision operator [33], although in the work of Ridenti *et al* [35] the Chapman–Cowling extension to the continuous approximation to rotations was developed to bridge the continuous energy loss regime applicable at high fields to the discrete collision description for use at low energies.

This work is arranged by first outlining our multi-term kinetic theory solution, and the Monte-Carlo code used for comparison with our results, in section 2. In section 3 we consider two systems that exhibit NDC—a simple model system in section 3.1 and N_2 in section 3.2. For both systems we present calculations of transport coefficients at various temperatures, and discuss the thermal activation of NDC and the necessity of de-excitation, or superelastic, collisions for its occurrence. As part of our model simulations for NDC, in section 3.1.3 we also consider a non-physical modification to our model system, to highlight the superelastic contribution. The prediction of NDC using Robson's [19] criterion from knowledge of the energy transfer rates is presented for both systems, in sections 3.1.2 and 3.2. As part of our benchmarking against the Monte-Carlo code, we assess the effect of the neglect of recoil in the Frost-Phelps differential finite difference inelastic collision operator [33], in section 3.1.1. Finally, in the Appendix, we also consider the effect of anisotropy in low-threshold inelastic collision channels of our model cross-section, and the neglect of higher order de-excitations sometimes applied in the solution of similar problems.

2. Theory

2.1. The Boltzmann equation and a multi-term solution framework

The transport of a swarm of charged particles through a gaseous medium is described by the particle phase space distribution function $f(\mathbf{r}, \mathbf{v}, t)$, representing the distribution of electrons with position $\mathbf{r}$, velocity $\mathbf{v}$ and time t, that is the solution of the linear Boltzmann equation,

$$\left(\frac{\partial}{\partial t} + \mathbf{v} \cdot \nabla + \frac{q\mathbf{E}}{m_e} \cdot \frac{\partial}{\partial v}\right) f(\mathbf{r}, \mathbf{v}, t) = -J(f(\mathbf{r}, \mathbf{v}, t)),$$

(1)

where m_e is the mass of the swarm particle, q is the elementary charge, and $\mathbf{E}$ is the externally applied electric field. The linear collision operator J describes binary collisions between the swarm particles and the background medium, and accounts for elastic and inelastic collisions, and particle non-conserving loss (attachment) and gain (electron impact ionisation) collisions.

For a solution to the Boltzmann equation, the angular dependence of the phase space distribution function is expanded in terms of spherical harmonics, to give:

$$f(\mathbf{r}, \mathbf{v}, t) = \sum_{l=0}^{\infty} \sum_{m=-l}^{l} f_m^{(l)}(\mathbf{r}, v, t) Y_m^{[l]}(\hat{\mathbf{v}}). \quad (2)$$

In practice, the index l must be truncated at some upper value l_{max}, incremented until some convergence criterion on the distribution function, or its velocity moments, is met. For this work we do not restrict the truncation at $l_{max} = 1$, as is commonly done for the 'two-term approximation', sometimes leading to an inadequate representation of the anisotropic parts of the distribution function and incorrect transport coefficients, see the review [34].

In plane parallel geometry, the preferred direction is taken to be perpendicular to the electrodes and the spatial gradients are along the z axis so that $\mathbf{r} = z$ and $\mathbf{E} = E_z$, and the m index is restricted to $m = 0$ by symmetry, so that $f_m^{(l)}(\mathbf{r}, v, t) = f_l(\mathbf{r}, v, t)$. Equation (1), with substitution of the expansion (2) and recast in energy-space using $qU = \frac{1}{2} m_e v^2$ for U in eV, becomes the system of coupled equations for $f_m^{(l)}$ [36]:

$$\frac{\partial f_l}{\partial t} + J_l(f_l) + \left(\frac{2q}{m_e}\right)^{1/2} \sum_{p=\pm 1} \Delta_l^{(p)} \left[U^{1/2}\frac{\partial}{\partial z}\right.$$
$$\left. + E_z\left(U^{1/2}\frac{\partial}{\partial U} + \frac{p}{2}\left(l + \frac{3p+1}{2}\right)U^{-1/2}\right)\right] f_{l+p} = 0,$$

$$\Delta_l^{(+)} = \frac{l+1}{2l+3},$$

$$\Delta_l^{(-)} = \frac{l}{2l-1},$$

(3)

where J_l is the Legendre decomposition of the collision operator, detailed in the next section, and E_z is the electric field defined parallel to the z axis.

2.2. Collision operators

For electron swarms in atomic and molecular gases the small mass ratio is utilised so that the Davydov operator for elastic collisions may be used [37–39]. The electron-impact ionisation operator, in the Legendre-decomposed form utilised here, is detailed in references [40, 41].

For inelastic, particle-conserving collisions, the Frost and Phelps Legendre-decomposed collision operator [33] is employed here. The anisotropic form of the collision operator was detailed by Makabe and White [42], Phelps and Pitchford [43] and earlier in Reid [44] (in the second and third terms on the right hand side of the equation following equation (3)), and is here extended to include de-excitation, or superelastic, collisions using detailed balance [45]. Expressed in terms of initial and final internal states j and k of the neutral particle, where $j < k$, particles with energy above the threshold U_{th} are available for excitations from $j \to k$. Below the threshold, for non-zero temperatures, the background neutral particles may be in an excited state k and are available to undergo superelastic collisions from $k \to j$, where the energy loss, taken to be the threshold, is gained by the incoming electron and lost by the neutral particle.

The partial cross-sections σ_l are the coefficients of a Legendre polynomial (P_l) expansion of the differential cross-sections, $\sigma(U, \chi)$ for the scattering angle χ, defined by $\sigma_l(U) = 2\pi \int_{-1}^{1} \sigma(U, \chi) P_l(\cos \chi) d(\cos \chi)$. The de-excitation cross-section $\sigma_l(kj; U)$ is expressed in terms of the excitation cross-section $\sigma_l(jk; U)$ using the microscopic reversibility relation $g_k U\sigma_l(kj; U) = g_j(U + U_{th})\sigma_l(jk; U + U_{th})$ where g_k and g_j are the degeneracy of the kth and jth states. After converting to collision frequencies through $\nu_l(U) = n_0 v \sigma_l(U) = n_0\sqrt{(2qU/m_e)}\sigma_l$ in energy space, where n_0 is the neutral number density, the isotropic and anisotropic components of the inelastic collision operator are given by:

$$J_0^{\text{inel}} = \sum_{j,k} n_{0j}\left\{\left(\frac{U + U_{th}}{U}\right)^{1/2} f_0(U + U_{th})\right.$$
$$\times \nu_0(jk; U + U_{th}) - f_0(U)\nu_0(jk; U)\Big\}$$
$$+ \sum_{j,k} n_{0k}\frac{g_j}{g_k}\left\{f_0(U - U_{th})\nu_0(jk; U)\right.$$
$$\left. - \left(\frac{U + U_{th}}{U}\right)^{1/2} f_0(U)\nu_0(jk; U + U_{th})\right\}, \quad (4)$$

$$J_{l\geqslant 1}^{\text{inel}} = \sum_{j,k} n_{0j}\left\{\left(\frac{U + U_{th}}{U}\right)^{3/2} f_l(U + U_{th})\right.$$
$$\times \nu_l(jk; U + U_{th}) - f_l(U)\nu_0(jk; U)\Big\}$$
$$+ \sum_{j,k} n_{0k}\frac{g_j}{g_k}\left\{\left(\frac{U - U_{th}}{U}\right) f_l(U - U_{th})\right.$$
$$\times \nu_l(jk; U)$$
$$\left. - \left(\frac{U + U_{th}}{U}\right)^{1/2} f_l(U)\nu_0(jk; U + U_{th})\right\}, \quad (5)$$

where ν_l is the lth partial collision frequency, related to the momentum-transfer cross-section through $\sigma_m = \sigma_0 - \sqrt{\frac{U + U_{th}}{U}} \sigma_1$ for inelastic collisions. The number density of the neutral particles in the initial and final states j and k, are n_{0j} and n_{0k}, respectively, calculated using standard Boltzmann statistics: $n_{0j} = \frac{n_0}{Z} g_j \exp\left(\frac{-U_j}{k_B T_0}\right)$. The partition function sums over all possible internal states j with energy U_j, and is given by $Z = \sum_j g_j \exp\left(\frac{-U_j}{k_B T_0}\right)$, where k_B is Boltzmann's constant and T_0 is the temperature of the neutral particles.

2.3. Solution technique

2.3.1. Time-of-flight. When the number density varies slowly in space, away from boundaries and under the influence of a uniform electric field, hydrodynamic conditions prevail and the space-time dependence of the distribution function can be projected onto the number density so that $f_l(z, U, t) = \sum_s f_l^s(U) \frac{\partial^s n(z,t)}{\partial z^s}$, where s is the rank of the tensor.

For weak gradients, a density gradient expansion of the phase-space distribution function may be taken to second order to account for particle non-conserving processes. The diffusion equation is then used to analyse experimental parameters [46]. The time-of-flight coefficients of the density gradient expansion are found from the solution to the hierarchy detailed in [47].

Knowledge of the full phase-space distribution function f allows for the calculation of all macroscopic quantities describing the electron swarm, as detailed in [46, 47]. An important self-consistency check for an accurate solution are the rates of energy and momentum exchange, where the gain from the advective terms (the external electric field and time rate of change components) and loss due to collisions must be balanced. Calculation of energy and momentum-transfer rates due to individual cross-sections allows assessment of the contribution of not only each collision type, but separation into inelastic and superelastic channels.

2.3.2. Numerics and benchmarking. Systematic benchmarking of the theory and numerical solution has been performed, with the particular numerical methods employed in the solution of equation (3) detailed in references [48, 49]. Here, linear interpolation of the tabulated cross-sections is employed, with a non-uniform energy grid that is denser at lower energies, in order to capture the variations near the low-energy thresholds of the inelastic processes considered throughout this work. The energy range of the simulation, U_∞, is chosen so that the distribution function captures the full energy range of the electron swarm, so that $f_0(U_\infty)/\max[f_0(U)] \leqslant 10^{-10}$. Using this condition, both the energy and momentum transfer rates are balanced to within $\pm 0.01\%$ for our simulations. For our multi-term solution, the $l_{\max}$ index and number of solutions nodes are

incremented until convergence in the distribution function, or its moments, is achieved to better than 0.1%.

2.4. Monte-Carlo technique

We have implemented a standard swarm Monte-Carlo sampling code. The code uses the null-collision method [50] along with temperature included via appropriate modifications to the total cross-section and resolution of collisions [51]. Measurements are made through the 'box sampling' style [52], where an integral over the quantities to be measured is performed between each collision and binned into time bins. Hence a time-specific measurement refers to an average of that quantity during the time bin. To ensure we have considered a large enough simulation time to have reached steady-state, we consider a sufficiently fine time grid to allow a fit of the quantities to the empirical form of: $x(t) = x_S + e^{-\lambda_x(t - T/2)}\delta x$, where x_S is the steady state value for quantity x and T is the final time of the simulation. This definition allows us to give δx the meaning of a deviation from steady-state at the half-way point of the simulation. The condition, $\delta x/x_S < 10^{-4}$ is enforced, and we then average over the latter half of the simulation to build up the statistics for the Monte-Carlo results.

We estimate the error in these results by the standard error of the averaged simulations at different times. We have also ensured that the autocorrelation between consecutive points is minimal.

The Monte-Carlo code has been tested against many benchmarks including pure elastic models of hard sphere and Maxwell models [53], argon measurements [49], the inelastic and anisotropic models of Reid [44, 53], the ionisation models of Ness and Robson [41, 53], and inclusion of a static structure factor [54].

As part of the tests to be performed in section 3.1.3, we require a different temperature for the elastic and inelastic processes. We have implemented this by considering a mixed system of two species. The first species possess only an elastic process, with a gas temperature given by the elastic temperature. The second species possesses only an inelastic process, with the ground and excited populations given by the inelastic temperature. When the elastic and inelastic temperatures coincide, this is equivalent to a simulation of a single species with both processes.

3. Results and discussion

3.1. NDC—a model cross-section study

The motivation for our model study is two-fold. Firstly is to use a simple analytic model cross-section set to understand the physical processes involved in NDC. Secondly, is in verifying the inclusion of (isotropic and anisotropic) superelastic processes in the inelastic channel. In the absence of superelastic processes, thermal temperatures cannot be achieved, so a simple model system, verified by an independent Monte-Carlo method, allows

us to confirm that our solution methods are well representing physical processes.

In the pursuit of clear criteria for the existence or prediction of NDC, a number of model cross-sections have been proposed (see for example [1]). Many of these models could be adapted to account for the inclusion of superelastic processes. The model considered in this work, however, was chosen to illustrate the damping effect of superelastic collisions on NDC at room temperature, similar to the behaviour of electrons in N_2. For collisions with neutrals with a mass $m_0 = 28$ amu, at 0 K, 77 K, and 293 K the transport coefficients have been calculated for the model elastic and excitation cross-sections (in atomic units):

$$\sigma_m^{elas} = A + BU,$$
$$\sigma_0^{inel} = \begin{cases} 0 & U \leqslant 0.002 \text{ eV}, \\ A & U > 0.002 \text{ eV}, \end{cases} \tag{6}$$

where $A = 1 \text{ Å}^2$ and $B = 5 \text{ Å}^2/\text{eV}$.

3.1.1. Drift velocity and recoil. Figure 1 shows the drift velocity and mean energy calculated using the multi-term Boltzmann equation solution and the independent Monte-Carlo code, as a function of the reduced electric field E/n_0 in units of the Townsend (1 Td = 10^{-21} Vm^2). The agreement between the Monte-Carlo and Boltzmann solutions is better than 1.4% for the drift velocities and the mean energies at 0 K, and with less than a 3.2% variation in the transport coefficients at 77 K. However, this increases to 5.6% for both the drift velocity and mean energy at 293 K.

To address some of the discrepancy between the transport coefficients calculated using our Boltzmann and Monte-Carlo solutions, we consider the neglect of recoil in the inelastic channel in our solution (and similar solutions of the Boltzmann equation, for example the recent work of Ridenti *et al* [35] in the continuous energy loss approximation). Unlike elastic collisions, that are represented to first order in the mass ratio to take into account the thermal motion and recoil of the neutral particle during an elastic collision, recoil of the neutral particle during inelastic collisions is neglected in many of the existing Boltzmann equation solutions, and in our solution. This assumption has been considered previously in White *et al* [55], using the integral form of the inelastic collision operator that does not restrict collisional representation to zeroth-order. In their study, the transport coefficients calculated for electron impact on H_2 using a multi-term solution over the range 0.1–10 Td, differed by less than 0.1% between no recoil inelastic collisions and the converged collision description. However, the lowest excitation channel in H_2 is the $0 \rightarrow 2$ rotational excitation with a threshold of 44 meV, while for our model system the energy loss threshold is 2 meV, closer to the first order mass ratio $\frac{m_e}{m_e + m_0} \approx 2 \times 10^{-5}$ for the model system.

To include the thermal motion of the neutrals during inelastic collisions in the Frost-Phelps differential finite difference collision operator [33], requires an extension that is outside the scope of this study. However, we still desire quantification of the effect on the transport coefficients. In
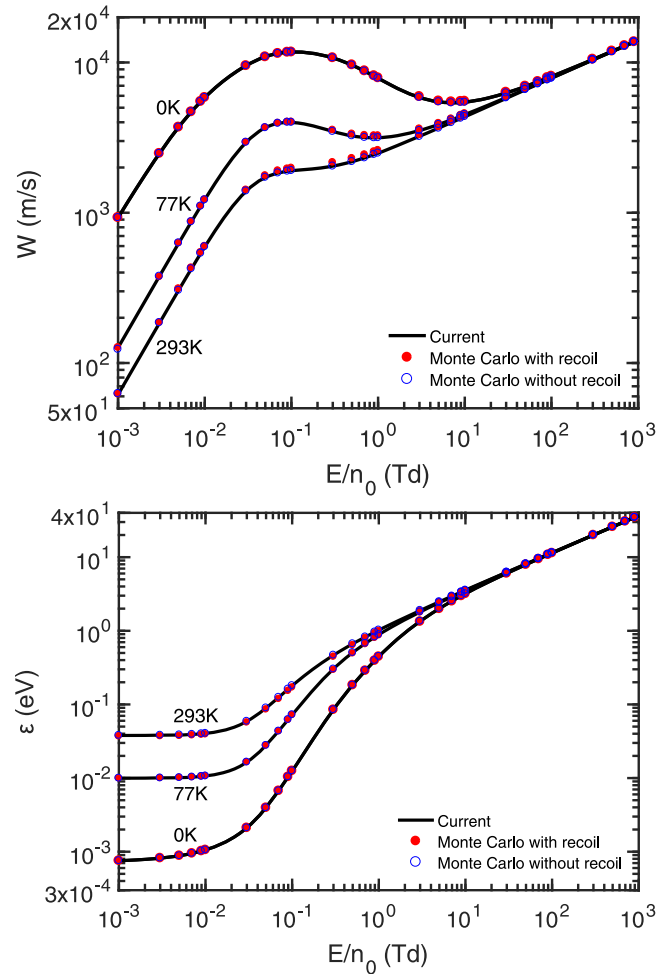

Figure 1. The calculated flux drift velocity (upper) and mean energy (lower) of a swarm of electrons whose collisional behaviour is described by the proposed model cross-section set, equation (6). The lines represent values calculated at various temperatures using the multi-term kinetic theory, while the symbols show the values calculated using an independent Monte-Carlo solution method. The solid red symbols represent the Monte-Carlo calculations treating inelastic collisions exactly, while the open blue symbols correspond to Monte-Carlo calculations with recoil of the neutral particle during inelastic collisions neglected.

Monte-Carlo simulations the collisions are treated exactly, so the Monte-Carlo technique described in section 2.4 was used to assess the effect of recoil in the low-threshold channel of interest here, as shown in figure 1. The effect of truncation of the mass ratio for inelastic collisions on our calculations is most prevalent at reduced electric fields between 0.1 Td and 10 Td, where the net energy transfer due to elastic collision is increasing relative to the energy transfer due to inelastic collisions, as shown in figure 2. Here, the difference between the complete and approximate collision descriptions in the Monte-Carlo calculations is greatest at 293 K, where the drift velocity and mean energy both differ by up to 6%. At 77 K the differences between the transport coefficients are up to 3%, while at 0 K the differences decrease to 1.6%, between the two collision representations.

When recoil of the neutral particle during inelastic collisions in our Monte-Carlo simulation is neglected by
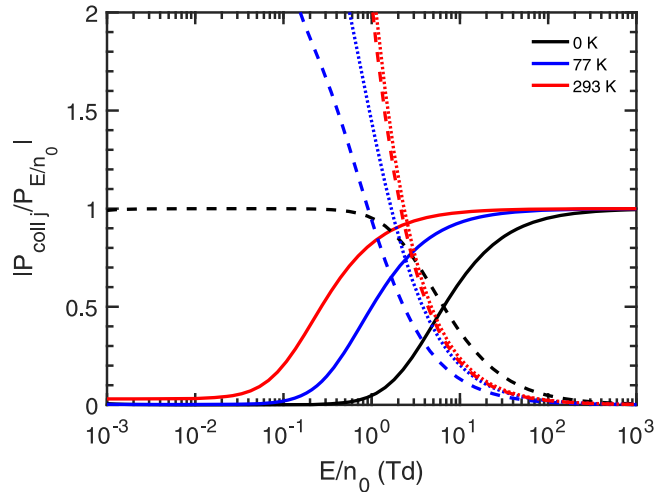
Figure 2. The energy transfer rates of each of the collision channels j of the model cross-section, equation (6), as a fraction of the power input from the external reduced electric field, at different temperatures, as a function of the reduced electric field. The solid lines show the fractional power transfer rates of the elastic collisions, the dashed lines represent the ground-state inelastic process, and the dotted lines represent the gain in energy due to the superelastic process only.

artificially increasing the neutral mass for inelastic collisions only, to replicate the differential finite difference form of the inelastic collision operator utilised here [33], the difference between our Monte-Carlo and Boltzmann calculations reduces to 0.4% and 0.3% for the drift velocity and mean energy, respectively, at 0 K, 0.6% between both the drift velocity and mean energy at 77 K, and below 0.7% between the drift velocities and 0.3% between the mean energies at 293 K.

3.1.2. NDC and Robson's criterion. The presence of NDC is anticorrelated with the presence of superelastic collisions, highlighting the damping effect of the de-excitation process on the presence of NDC. When properly included through detailed balance for inelastic collisions, a smaller ratio of neutrals in the ground-state, caused by an increasing temperature, increases the mean energy of the swarm and decreases the drift velocity. The energy transfer profiles given in figure 2 show the lower net inelastic energy transfer rate with increasing temperature, increasing the mean energy which samples higher-energy regions of the elastic cross-section, resulting in a reduced average velocity of the swarm. NDC ceases when the collisional energy transfer is dominated by the elastic process. At higher temperatures, the increased fraction of neutrals in excited-state populations reduces the net power transfer due to inelastic collisions, as shown by the superelastic contribution to the energy transfer in figure 2. As a direct result of the temperature and the resulting number of neutral particles in an excited state, the range of NDC is reduced and the transition to elastic-collision dominated

energy transfer occurs at lower reduced electric fields for increasing temperatures.

Using momentum-transfer theory, Robson's [19] criterion for the presence of NDC uses the energy variation of the ratio of the elastic to inelastic energy transfer. The criterion derived for the appearance of NDC by Robson [19], at a particular mean energy ε, is given by $1 + \frac{\partial \Omega}{\partial \varepsilon} < 0$ where Ω represents the ratio of the total inelastic to elastic energy transfer and is given by:

$$\Omega \equiv \frac{\sum_j U_{th}^j \{\langle \nu_0^{\text{inel},j}(jk; \varepsilon) \rangle - \langle \nu_0^{\text{inel},j}(kj; \varepsilon) \rangle \}}{\frac{2m_e}{m_0} \langle \nu_m^{\text{elas}}(\varepsilon) \rangle}, \quad (7)$$

where the total inelastic energy transfer is taken as the sum over all inelastic channels j with associated thresholds U_{th}^j.

We note that the NDC criteria of Robson [19] and Petrović *et al* [1] differ due to a different expression for the energy balance, where the latter omit energy transfer due to elastic collisions, although this is sufficient for the systems considered in that work.

The criterion proposed by Robson [19] is a very good predictor for NDC for the model cross-section considered in this study, as shown in figure 3. For a monotonically increasing elastic collision frequency and open inelastic channels, the mean energy increases with increasing E/n_0, slowly as the inelastic collisions take energy from system, so that the drift velocity increases with field, as illustrated in figure 1. As the inelastic collisions become less important relative to the elastic collisions, the mean energy of the swarm increases at a greater rate, to sample the higher elastic collision frequency, causing the drift velocity to begin to decrease with increasing field. The NDC region for 0 K and 77 K ceases when the energy transfer rate due to elastic collisions is greater than the net energy transfer rate due to the inelastic process, as predicted. For the calculation of Ω at 293 K, for reduced electric fields between 0.1 Td and 0.2 Td, the derivative is ≈ -1 and the presence of NDC is only weakly predicted, but does not occur in our calculations.

3.1.3. Temperature dependence and detailed balance. To illustrate the physical dependence on the inclusion of superelastic collisions, in this subsection we consider two unphysical modifications to our model system. These address the effect of temperature from each of the scattering channels separately by setting different temperatures for the background gas through elastic collisions and excited state populations.

The first modification includes temperature dependence of the excited state population, but considers elastic collisions with stationary neutrals, equivalent to a temperature of 0 K in the elastic collision operator, with the notation $J^{\text{elas}} = 0$ K, $J^{\text{inel}} = 293$ K in the following figures. The second modification involves elastic collisions with non-stationary neutrals, at 293 K, but inelastic collisions from ground- to excited-states only, with the notation $J^{\text{elas}} = 293$ K, $J^{\text{inel}} = 0$ K in figures 4–5.
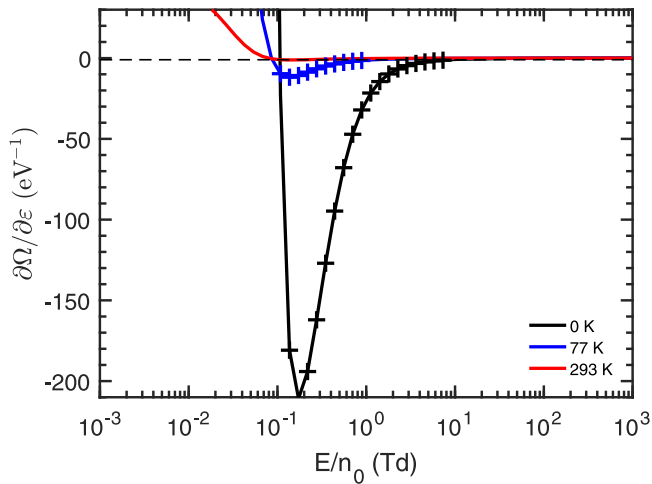
Figure 3. Rate of change of Ω with mean energy as a function of the reduced electric field, for a swarm of electrons whose collisional behaviour is described by our model cross-sections of equation (6). The solid lines show $\partial\Omega/\partial\varepsilon$ at varying temperatures, where below -1 (indicated by the dashed horizontal line) NDC is predicted by Robson's criterion [19]. The symbols indicate where NDC is present in our calculated drift velocity. We note that the prediction of NDC at 0 K appears to occur earlier than its appearance in the calculated data; however, this is only due to the rapid decrease in the derivative around 0.1 Td.

Figure 4 displays the mean energy from our Boltzmann solution and our independent Monte-Carlo solution. Here, in our Monte-Carlo simulation inelastic collisions were treated exactly.

For properly included superelastic collisions, but when temperature is not included in the elastic channel, the mean energies approach the appropriate thermal value of $\approx \frac{3}{2}k_B T_0$ with decreasing E/n_0. At 293 K a difference of around 3.6% between the non-physical model and standard model calculation is observed, generally decreasing with increasing E/n_0. We find that the drift velocity calculations (not shown) lie very close to, but just above, the standard model calculations at 293 K, by at most 2.2%. While those differences are not as significant as some of the others discussed in this study, these calculations do illustrate the importance of detailed balance in swarm calculations for achieving correct thermal distributions.

A more dramatic difference is observed when temperature effects are taken into account for the elastic collisions, but not in the inelastic channel. Here, the calculated drift velocity and mean energy approach the 0 K calculations due to the dominance of the inelastic channel at low reduced electric fields, as can be seen in the energy transfer profiles given in figure 5. The difference between this non-physical modification and the 0 K profile of figure 1 shows the explicit contribution of the temperature term in the elastic collision operator, where the mean energy lies up to 5% below the standard 0 K calculations, and the drift velocity differs by up to 4%, both greatest at the lowest E/n_0. The variation from the standard temperature treatment profile is large, and results in an overestimate of the drift velocity below 30 Td, mimicking the 0 K drift velocity profile of figure 1, and the
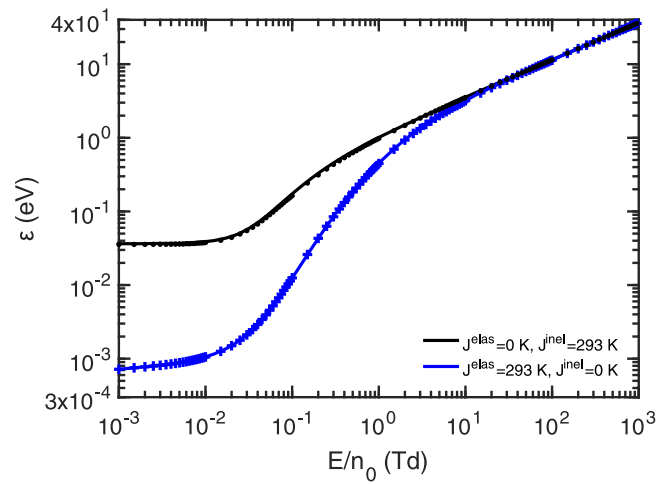

Figure 4. The calculated mean energy of a swarm of electrons whose collisional behaviour is described by the proposed model cross-section set. The lines represent values calculated for the various models using the multi-term kinetic theory solution, while the symbols correspond to values calculated using an independent Monte-Carlo method, where the same colour denotes the same model. See text for details of the model notation.
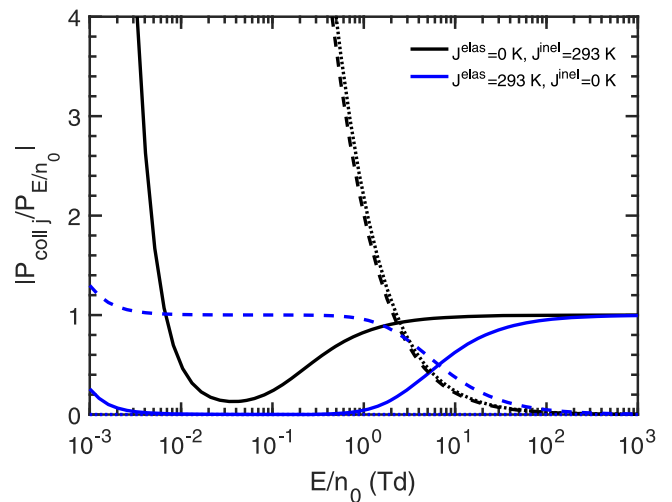

Figure 5. The energy transfer rates for each of the collision channels of the model cross-section, with varying reduced electric fields, as a fraction of the power input from the external reduced electric field. The line-styles here are the same as described in figure 2.

presence of an NDC region that is larger than that in the standard 77 K calculations and absent from the 293 K calculations.

When temperature effects are included through the elastic collision operator and the inelastic ground-state density, but detailed balance is not achieved due to the neglect of superelastic collisions altogether, we observe a dramatic effect on the transport coefficients, given the large contribution of the de-excitation process to the energy transfer. Although not shown, the resulting drift velocity and mean energy profiles lie between the 0 K and 293 K results. This is to be expected with less energy lost in the inelastic channel than the 0 K simulation, but a greater net energy loss in the inelastic channel than the 293 K simulation, where the
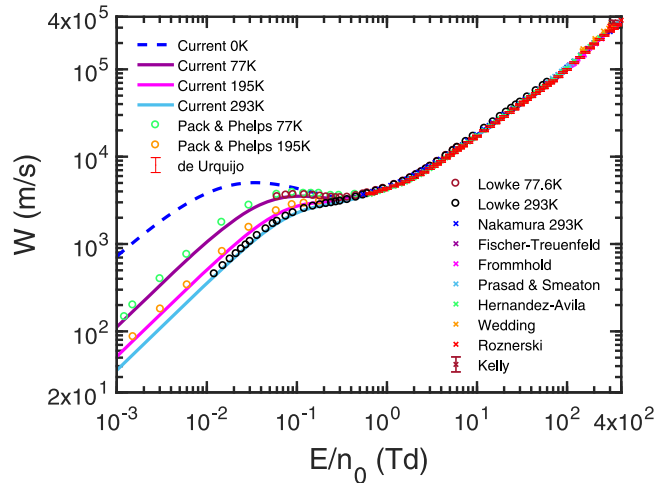
Figure 6. Comparison of the calculated drift velocity for an electron swarm in N_2 as a function of reduced electric field, with some of the other available experimental measurements at various temperatures. Our calculations at 0 K, 77 K, 195 K, and 293 K, depicted by the solid lines, are compared with the experimental measurements of Pack and Phelps at 77 K and 195 K [21, 22], de Urqujio *et al* [59], Lowke at 77.6 K and 293 K [32], Nakamura at 293 K [60], Fischer-Treuenfeld [61, 62], Frommhold [63, 64], Prasad and Smeaton [65, 66], Hernández-Ávila *et al* [67], Wedding *et al* [68], Roznerski [69, 70], and Kelly [71] (digitised from Campbell *et al* [72]).

Figure 7. The net power transfer rate for N_2 for each collision type, as a fraction of the advective power transfer, for electron impact at 77 K (dashed lines) and 293 K (solid lines), as a function of E/n_0. The coloured lines correspond to: black—elastic, dark blue—rotational excitations, light blue—superelastic rotational processes, red—vibrational excitations, dark red—superelastic vibrational processes, purple—other excitations, and orange—ionisation. The power transfer for the inelastic channels have been grouped by type (rotations, vibrations, etc.) for the figures only. The fractional power transfer in the rotational channel at 77 K is slightly larger in magnitude than at 293 K, although this is almost indistinguishable on the figure. The power transfer in the ionisation and other excitation channels (excluding rotations and vibrations) are the same at both temperatures, where the transport coefficients at those E/n_0 for all temperatures have converged.

de-excitation collisions contribute to energy gained by the electron swarm. These model systems highlight the necessity of detailed balance in collisional processes when modelling real gaseous systems in the low energy regime.

For these non-physical models, which disregard thermal effects in the elastic, inelastic and superelastic channels, NDC is present in our results for the two cases where the de-excitation process is removed. Similar to the results discussed in section 3.1.2, the presence of superelastic collisions increases the mean energy of the electron swarm, increasing the drift velocity monotonically. As demonstrated by the earlier results, Robson's criterion for the presence of NDC gives a very accurate prediction based only on a knowledge of the energy transfer rates. Regardless of the temperature of the model system, in the absence of the de-excitation process the ratio of the energy transfers in equation (7) decreases more rapidly with energy than it would otherwise, resulting in NDC until the elastic energy transfer rate starts to dominate.

3.2. NDC in N_2

For application of our discussion of the temperature dependence of NDC to real gases, both experimental measurements and simulations provide a clear illustration of the effect in N_2. As shown in figure 6, in N_2 an NDC region is present in the measurements of both Pack and Phelps [21, 22] and Lowke [32] at 77 K and 77.6 K, respectively. All of the experimental measurements show an absence of NDC at 293–300 K. Our calculations, using the cross-section set of Biagi [56–58] outlined in [59], along with the calculations of Frost and Phelps [33] and Petrović *et al* [1], are in good agreement with the experimental measurements of these authors.
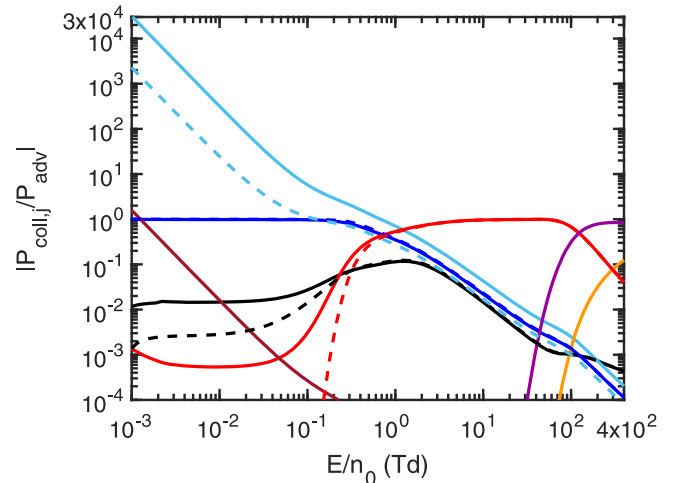
An increase in the drift velocity and the appearance of an NDC region occurs in the absence of superelastic processes. Highlighted in the work of Petrović *et al* [1] is the importance of superelastic collisions for both the low-threshold rotational and vibrational excitation channels. As with our model cross-section, the temperature dependence of the excited state populations in N_2, and the reduced net energy transfer due to inelastic collisions, compared to the 0 K calculations, is responsible for the absence of NDC at 195 K and 293 K. At 77 K, the decreased population of the excited states for rotational and vibrational excitations results in a higher net energy transfer rate in those channels, and a corresponding decrease in the drift velocity with increasing E/n_0.

In figure 7 the power transfer rates calculated for each collision type are given for 77 K and 293 K only. The explicit power transfer due to the de-excitation processes (in particular rotational excitations) illustrate that the increased contribution of the superelastic processes at the higher temperatures, adding energy to the swarm, is responsible for the decreased range and eventual disappearance of the NDC region. The resulting increased mean energy of the swarm changes the sampled region of the elastic collision frequency, causing an increased drift velocity. The temperature dependence of the NDC region has been observed previously through the variation of the vibrational channel temperature, at a fixed neutral gas temperature, in mixtures of 99% argon and 1% N_2 in [26]. Our present work illustrates the same dependence of NDC
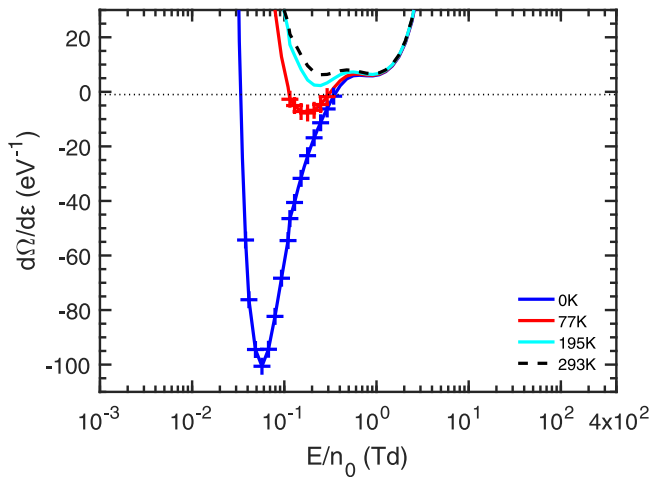
Figure 8. Rate of change of Ω with mean energy as a function of reduced electric field for electrons in N_2. The solid lines show $\partial\Omega/\partial\varepsilon$ calculated from the energy transfer rates for N_2 at varying temperatures, where NDC is predicted by Robson's criterion when $\partial\Omega/\partial\varepsilon < -1$ [19] (shown by the horizontal dotted line). The symbols indicate where NDC is present in our calculated values.

occurring in a pure gas, although here the neutral gas temperature is varied to change the rotational populations.

The calculation of Robson's NDC criterion [19] at each temperature is a very good predictor for the presence of NDC in N_2 also. Observed at 0 K and 77 K, figure 8 shows that the prediction of NDC using the criterion $\partial\Omega/\partial\varepsilon < -1$ was consistent with our calculations. Our new experimental measurements are also in very good agreement with these predictions. At 293 K, although close, the experimental data do not exhibit NDC.

4. Concluding remarks

In this study we have investigated the temperature dependence of NDC using a simple model system, alongside that of N_2. The power transfer rates in the elastic, inelastic and superelastic channels show the damping effect of the de-excitation processes on the range of NDC. With increasing temperatures, the higher proportion of neutral background gas particles in excited states increases the mean energy and subsequently suppresses the NDC region that arises from the increasing elastic momentum-transfer cross-section compared with the (decreasing importance of the) inelastic channels at those fields.

To assess the impact of superelastic collisional processes on NDC, we employed some model (although unphysical) cases, with temperature dependence during elastic, excitation and de-excitation processes manipulated. These have illustrated the importance of the de-excitation process to the transport coefficients at low reduced electric fields. These systems also isolated the physical processes responsible for NDC, with the energy gained by the electron swarm from the de-excitation channel reducing the range of, or eliminating NDC altogether.

We have also presented calculations of Robson's [19] criterion for the presence of NDC using the rate of change of the

ratio of the net energy exchange of inelastic to elastic collisions, derived using momentum transfer theory. That criterion predicts well the region of NDC in all of the model cases considered, as well as the temperature-dependent NDC region present in N_2, using only a knowledge of the collision frequencies.

In the Frost-Phelps [33] differential finite difference form of the inelastic collision operator utilised in this work, the representation of inelastic collisions is truncated at zeroth order in the mass ratio, neglecting the recoil of the neutral particle during an inelastic collision. The effect of this assumption had been assessed previously and found to have less than a 0.1% impact on the calculated transport coefficients for electrons in H_2 [55]. For the model cross-section considered in this work, however, the inelastic threshold is more than 20 times lower than the lowest rotational threshold in H_2, and the impact of the truncation of the mass ratio for inelastics was found to have a greater influence on the transport coefficients. At 0 K recoil accounts for a less than 2% change in the drift velocity and mean energy, but this difference increased to over 6% at room temperature. To derive the next terms in the mass ratio expansion for the Frost-Phelps inelastic operator was beyond the scope of the present work, however should be considered when adjusting cross-sections derived from swarm transport measurements for processes with very low thresholds (for example, the derived vibrational cross-sections for H_2 [55, 73]).

The effect of anisotropic scattering, for very-low threshold inelastic processes on the transport coefficients, was assessed using a model cross-section to replicate the forward-peaked nature of rotational collisions. The inclusion of an inelastic momentum-transfer cross-section results in a 5%–11% increase in the drift velocity, and between a 4% and 9% change in the mean energy of the electron swarm for the temperatures considered in this work, as detailed in the Appendix.

Finally, our calculations for an electron swarm in N_2 for temperatures between 0 and 293 K were used to illustrate the physical processes associated with NDC and the effect of temperature on its appearance or absence, with the same dependence on the gas temperature and number of neutrals in an excited state found as in our model calculations.

Acknowledgments

Appendix: Approximation effects: anisotropy in the inelastic channel, higher-order superelastic processes, and the two-term approximation

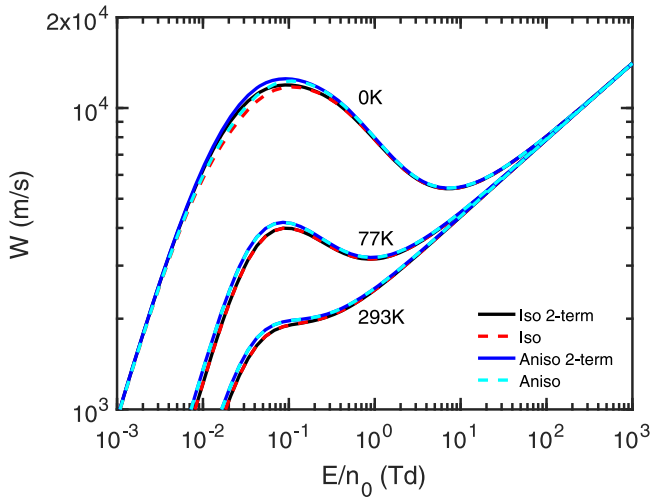In this appendix we quantify the effect of various approximations on both our model cross-section set and on N_2.

Figure A1. Variation of the drift velocity with reduced electric field for the scattering model detailed in equations (6) and (A1), at different temperatures. Results are shown for a two-term approximation (labelled 2-term), multi-term calculation for the isotropic model (labelled Iso) and anisotropic scattering in the inelastic channel (labelled Aniso).

These include anisotropy in very low threshold inelastic processes, the two-term approximation, and the absence of superelastic processes in the $l \geqslant 1$ equation of the inelastic collision operator.

A.1. Model cross-section

In this study we are interested in the effect of anisotropic scattering in low-threshold processes like rotational excitations. The impact on the calculated transport coefficients are explored in this subsection, alongside our assessment of other assumptions.

The effect of anisotropic scattering in the inelastic channel has been recently investigated in Janssen *et al* [74], for an excitation scattering channel of (simplified) argon with a threshold at 11.828 eV. We note this energy threshold is much higher than the lowest inelastic thresholds of molecules like N_2. For the low threshold processes considered here, to quantify the effects of the anisotropic terms in the inelastic operator, given in equations (4) and (5), we introduce an angular scattering component for our model excitation in order to emulate the forward-peaked nature of rotational excitations. Using a forward scattering model, similar to the pronounced forward and back scattering model of Reid [44], we have selected the differential inelastic cross-section to be $\sigma^{inel}(U, \chi) \propto \cos(\chi/2)$, so that the inelastic momentum-transfer cross-section is given by:

$$\sigma_m^{inel} = \frac{4}{5}\sigma_0^{inel}. \qquad (A1)$$

To test explicitly the assumption of isotropic scattering in the inelastic channel, here we modify only the inelastic momentum-transfer, leaving the total inelastic and elastic momentum-transfer cross-sections fixed, as has been considered previously by Reid [44] and Phelps and Pitchford [43], for example. Note that this does not fix the total momentum-

transfer cross-section. Our calculated drift velocities for the anisotropic model combining equations (6) and (A1) are shown in figure A1. For the various temperatures considered in this work, the effects of anisotropy in the inelastic channel are greatest where momentum exchange is dominated by the inelastic channel. At 0 K, this difference occurs over the range 0.02–0.2 Td with a variation of less than 5% in the drift velocity and less than 9% in the mean energy of the swarm (not plotted). For the 77 K and 293 K simulations, the maximum difference occurs at the lowest reduced electric fields, where the momentum exchanged during superelastic collisions increases the total momentum exchanged in the inelastic channel. At 77 K the drift velocity and mean energy differ by 11% and 6.5% respectively, and 10% and 4% at 293 K, respectively, decreasing with increasing E/n_0 for both temperatures.

The validity of using a two-term approximation has been discussed previously (e.g. in [34, 43]), and we briefly consider the effects of that assumption on our model calculations here. Figure A1 shows our calculated drift velocity for isotropic and anisotropic scattering using the model cross-sections of equations (6) and (A1). For both the isotropic and anisotropic models, the difference between the two-term and multi-term results is greatest at 0 K, with a difference of up to 8% for $E/n_0 < 0.1$ Td in the drift velocity, and 5% in the mean energy. While at 77 K and 293 K, for both models, the differences between these transport coefficients reduces to below 0.3%.

The final assumption we wish to address is that while de-excitation is considered in the $l = 0$ equation of the inelastic operator, it is sometimes neglected in the $l \geqslant 1$ equations. For our isotropic model detailed in equation (6), we have removed superelastic collisions in the $l \geqslant 1$ channels in two ways. First we consider the proportion of particles in the ground-state calculated according to the neutral temperature, as is included through the $l = 0$ equation, but simply turn off the de-excitation channel. The differences between the calculated drift velocity and mean energy, when compared with our standard treatment, are up to 33% and 16% at 77 K and 30% and 10% at 293 K, respectively. We also considered neglecting higher-order superelastic terms by setting all neutral particles in the ground state, and find much smaller differences as the total number of excitation collisions remains constant, with differences of less than 9% and 1% in the drift velocity and mean energy, respectively, at 77 K, and 2% and 0.3% at 293 K. The magnitude of these differences decreases with increasing E/n_0, influenced by the relative strength of the two cross-sections, and the dominance of the elastic cross-section above 1 Td.

For each of the cases tested, our calculations demonstrate that significant differences can appear when various approximations are made, or detailed balance is neglected. The largest difference we calculated, and that was of particular interest in this study, was for anisotropic scattering in the low-threshold inelastic channel for our model system, where differences of up to 11% in the transport coefficients were calculated from the inelastically-isotropic model.

A.2. N_2

The impact of various approximations on the drift velocity for electron swarms in N_2 are detailed in this subsection.

In consideration of the differences between our calculations, using the cross-section set of Biagi [56, 57] as detailed in [59], and some of the experimental measurements, as detailed in de Urquijo *et al* [59], we have investigated the effect of l_{max} on the calculated drift velocity, specifically using a two-term solution, the limitations of which have been discussed in detail previously (e.g. [34]). The agreement with the de Urquijo *et al* [59] experimental measurements, shown in figure 6, is improved by using a two-term solution, with the errors decreasing from less than 2.8% from our multi-term calculations, to less than 2.6% for the two-term calculation results.

As part of our analysis of our calculations, we also consider the energy sharing fraction between the two post-collision electrons resulting from the ionisation process, taken here to be equally shared between the scattered and ejected electrons. At 360 Td, the highest reduced electric field considered in this work, we find a difference of less than 0.4% and 0.6% between the drift velocities and mean energies, respectively, from the 50%–50% sharing fraction and 1%–99% sharing fraction. Comparing the 50%–50% sharing fraction results with those for all-fractions being equiprobable, a less than 0.02% difference is calculated between the drift velocities, and less than 0.3% between the respective mean energies. The size of these differences is not unexpected given that the power transfer from the ionisation channel is of a similar magnitude to the (individual) excitations at the highest reduced electric field considered (see figure 7 where the power transfer of the ionisation process is compared with the grouped excitation power transfer (other than rotational and vibrational processes)).

We also note that the neglect of recoil in the inelastic channel in our solution may have some impact on our N_2 calculations, as in our model cross-section. The mass ratio and rotational threshold in the model are similar to those for N_2, and the power transfer rates show similar behaviour to the model calculations. This observation may be able to account for some of the underestimation of our calculated transport coefficients when compared with those from the present experiment.

Transport coefficients are dependent on how the experimental current trace is analysed [75, 76], so we have compared the calculated flux, bulk, and steady-state Townsend drift velocities to the drift velocity extracted from our pulsed Townsend experiment. It is expected that the differences between the various possible drift velocities increase with increasing E/n_0, with the particle non-conserving ionisation channel increasing in importance (as shown in the power transfer rates in figure 7). At the highest reduced electric field considered here, 360 Td, the difference between the flux and SST drift velocities is 2.5%, while a 10% difference is calculated between the bulk and flux drift velocities at this field.

Similar to the calculations of Frost and Phelps [33] and Petrović *et al* [1], where superelastic collisions were neglected in the rotational channel, or all excitation channels, respectively, we are interested in the effect of excluding de-excitation processes in the $l \geqslant 1$ terms of the inelastic collision operator,

but retaining their inclusion in the $l = 0$ term. In Frost and Phelps, neglecting rotational superelastic processes resulted in a change of 2% in the momentum-transfer collision frequency as a function of the characteristic energy, while in Petrović *et al* excluding all de-excitations results in a much greater change to the drift velocity. To quantify the effect on the drift velocity, unlike with our model calculations in section A.1, with only one excitation channel, in N_2 the scaling of the ground-state excitations, when modifying state populations, requires more consideration as the number of rotational channels significantly populated changes with the temperature of the neutrals. There are multiple scalings of the ground-state equation that may be considered (for example, with non-zero temperature or at 0 K, or with or without degeneracy considered), so we have assessed the two extreme possibilities combined with setting the number of neutrals in an excited state to zero for $l \geqslant 1$. We first consider using the proper ground-state density for n_{0j}, calculated using the neutral temperature, and secondly with no scaling at all (effectively $n_{0j} = 1$):

1. When the density of neutrals in the ground state are calculated according to the temperature of the neutrals, the difference from our standard 293 K calculations of the drift velocity changes by less than 4%. The difference decreasing with increasing E/n_0, as the higher threshold processes with lower excited-state densities (being neglected) starting to dominate.

2. For the extreme case of no temperature-dependent scaling or degeneracy included in the $l \geqslant 1$ equation, when setting $n_{0j} = 1$, this is not equivalent to the case considered in our model calculations with 0 K in the $l \geqslant 1$ equation of the inelastic operator. In this case, all of the rotational processes would be weighted equally, so the resulting transport would be influenced by the number of rotational cross-sections included in the set. In our current set of more than 40 individual rotational processes, the difference from our standard calculations and this modified set, results in an up to 60% difference in the drift velocity. The much higher number of neutrals in the ground state for each excitation channel results in higher momentum exchange with electrons with energies reduced to $U - U_{th}$, resulting in a reduced mean energy and drift velocity.

For both of these extreme cases, the neglect of superelastic processes has an important impact on the calculated transport coefficients, when considering the $\pm 0.1\%$ accuracy required in swarm calculations, and even the 10% error acceptable in plasma applications [34].

ORCID iDs

M J E Casey ⓘ https://orcid.org/0000-0003-0193-211X
D G Cocks ⓘ https://orcid.org/0000-0002-9943-7100
G J Boyle ⓘ https://orcid.org/0000-0002-8581-4307
S Dujko ⓘ https://orcid.org/0000-0002-4544-9106
J de Urquijo ⓘ https://orcid.org/0000-0003-3379-9843
R D White ⓘ https://orcid.org/0000-0001-5353-7440

References

[1] Petrović Z Lj, Crompton R W and Haddad G N 1984 *Aust. J. Phys.* **37** 23

[2] Dyatko N, Kochetov I and Napartovich A 2014 *Plasma Sources Sci. Technol.* **23** 043001

[3] Christophorou L G, McCorkle D L, Maxey D V and Carter J G 1979 *Nucl. Instrum. Methods* **163** 141

[4] Mathieson E and El Hakeem N 1979 *Nucl. Instrum. Methods* **159** 489

[5] Al-Dargazelli S S, Ariyaratne T R, Breare J M and Nandi B C 1981 *Nucl. Instrum. Methods* **176** 523

[6] Lopantseva G B, Pal A F, Persiantsev I G, Polushkin V M, Starostin A N, Timofeev M A and Treneva E G 1979 *Fiz. Plazmy* **5** 1370

[7] Christophorou L G (ed) 1981 *Electron and Ion Swarms: Proc. Second Int. Swarm Seminar, Oak Ridge, Tennessee, USA* (22–23 July, Oxford, Berkeley, CA: Pergamon, The University of California)

[8] Petrović Z Lj, Šuvakov M, Nikitović Ž, Dujko S, Šašić O, Jovanović J, Malović G and Stojanović V 2007 *Plasma Sources Sci. Technol.* **16** S1

[9] Nakamura Y 1995 *Aust. J. Phys.* **48** 357

[10] Long W H Jr, Bailey W F and Garscadden A 1976 *Phys. Rev. A* **13** 471

[11] Mirić J, Simonović I, Petrović Z Lj, White R D and Dujko S 2017 *Eur. Phys. J. D* **71** 289

[12] White R D and Robson R E 2009 *Phys. Rev. Lett.* **102** 230602

[13] Chiflikian R 1995 *Phys. Plasmas* **2** 3902

[14] Chiflikyan R 2000 *Phys. Plasmas* **7** 2704

[15] Šuvakov M, Petrović Z Lj, Marler J, Buckman S J, Robson R E and Malović G 2008 *New J. Phys.* **10** 053034

[16] Banković A, Dujko S, White R D, Marler J P, Buckman S J, Marjanović S, Malović G, García G and Petrović Z Lj 2012 *New J. Phys.* **14** 035003

[17] Banković A, Dujko S, White R D, Buckman S J and Petrović Z Lj 2012 *Nucl. Instrum. Methods Phys. Res.* B **279** 92

[18] Banković A, Dujko S, Marjanović S, White R D and Petrović Z Lj 2014 *Eur. Phys. J. D* **68** 127

[19] Robson R E 1984 *Aust. J. Phys.* **37** 35

[20] Vrhovac S B and Petrović Z Lj 1996 *Phys. Rev. E* **53** 4012

[21] Pack J L and Phelps A V 1961 *Phys. Rev.* **121** 798

[22] Pack J L and Phelps A V 1961 Dutton database, www.lxcat.net (Accessed: 03 January, 2018).

[23] Hunter S R, Carter J G and Christophorou L G 1985 *J. Appl. Phys.* **58** 3001

[24] Aleksandrov N, Dyatko N, Kochetov I, Napartovich A and Lo D 1996 *Phys. Rev. E* **53** 2730

[25] Donko Z and Dyatko N 2016 *Eur. Phys. J. D* **70** 135

[26] Dyatko N A, Ionikh Y Z, Meshchanov A V, Napartovich A P and Barzilovich K A 2010 *Plasma Phys. Rep.* **36** 1040

[27] Stano M, Pinhão N, Loffhagen D, Kučera M, Donkó Z and Matejčík Š 2011 *Eur. Phys. J. D* **65** 489

[28] Mirić J, Bošnjaković D, Simonović I, Petrović Z Lj and Dujko S 2016 *Plasma Sources Sci. Technol.* **25** 065010

[29] Kleban P and Davis H T 1977 *Phys. Rev. Lett.* **39** 456

[30] Kleban P and Davis H T 1978 *J. Chem. Phys.* **68** 2999

[31] Shizgal B 1990 *Chem. Phys.* **147** 271

[32] Lowke J J 1963 *Aust. J. Phys.* **16** 115

[33] Frost L S and Phelps A V 1962 *Phys. Rev.* **127** 1621

[34] White R D, Robson R E, Schmidt B and Morrison M A 2003 *J. Phys. D: Appl. Phys.* **36** 3125

[35] Ridenti M A, Alves L L, Guerra V and Amorim J 2015 *Plasma Sources Sci. Technol.* **24** 035002

[36] Robson R E, Winkler R and Sigeneger F 2002 *Phys. Rev. E* **65** 056410

[37] Davydov B I 1935 *Phys. Z. Sowj. Un.* **8** 59

[38] White R D and Robson R E 2011 *Phys. Rev.* E **84** 031125

[39] Pidduck F B 1936 *Q. J. Math.* **7** 199

[40] Ness K F 1985 Kinetic theory for charged particle swarms in gases with application to electron *PhD Thesis* James Cook University, Australia

[41] Ness K F and Robson R E 1986 *Phys. Rev. A* **34** 2185

[42] Makabe T and White R 2015 *J. Phys. D: Appl. Phys.* **48** 485205

[43] Phelps A V and Pitchford L C 1985 *Phys. Rev. A* **31** 2932

[44] Reid I D 1979 *Aust. J. Phys.* **32** 231

[45] Hochstim A R 1969 *Kinetic Processes in Gases and Plasmas* (New York: Academic) (https://doi.org/10.1016/B978-0-123-95615-6.X5001-2)

[46] Robson R E, White R D and Ness K F 2011 *J. Chem. Phys.* **134** 064319

[47] Robson R E and Ness K F 1986 *Phys. Rev. A* **33** 2068

[48] Boyle G J, Tattersall W J, Cocks D G, Dujko S and White R D 2015 *Phys. Rev. A* **91** 052710

[49] Boyle G J, McEachran R P, Cocks D G and White R D 2015 *J. Chem. Phys.* **142** 154507

[50] Skullerud H R 1968 *J. Phys. D: Appl. Phys.* **1** 1567

[51] Ristivojevic Z and Petrović Z Lj 2012 *Plasma Sources Sci. Technol.* **21** 035001

[52] Dujko S, White R D and Petrović Z Lj 2008 *J. Phys. D: Appl. Phys.* **41** 245205

[53] Boyle G J 2015 The Modelling of Non-equilibrium Light Lepton Transport in Gases and Liquids *PhD Thesis* James Cook University

[54] Tattersall W, Cocks D, Boyle G, Buckman S and White R 2015 *Phys. Rev. E* **91** 043304

[55] White R D, Morrison M A and Mason B A 2002 *J. Phys. B: At. Mol. Opt. Phys.* **35** 605

[56] Biagi S F 2012 Biagi Database (Magboltz version 8.97), http://lxcat.net/Biagi (Accessed: 03 January, 2018)

[57] Biagi S F 2017 Magboltz version 8.97, http://magboltz.web.cern.ch/magboltz/, (Accessed: 31 December 2017)

[58] Itikawa Y 2006 *J. Phys. Chem. Ref. Sata* **35** 31

[59] de Urquijo J, Casey M J E, Serkovic-Loli L N, Cocks D G, Boyle G J, Jones D B, Brunger M J and White R D 2019 *J. Chem. Phys.* **151** 054309

[60] Nakamura Y 1987 *J. Phys. D: Appl. Phys.* **20** 933

[61] Fischer-Treuenfeld W 1965 *Z. Phys.* **185** 336

[62] Fischer-Treuenfeld W 1965 Dutton Database, www.lxcat.net/Dutton, (Accessed: 03 January 2018)

[63] Frommhold L 1960 *Z. Phys.* **160** 554–7

[64] Frommhold L 1960 Dutton Database, www.lxcat.net/Dutton, (Accessed: 03 January 2018)

[65] Prasad A and Smeaton G 1967 *Br. J. Appl. Phys.* **18** 371

[66] Prasad A and Smeaton G 1967 Dutton Database, www.lxcat.net/Dutton, (Accessed 03 January 2018)

[67] Hernández-Ávila J L, Basurto E and de Urquijo J 2004 *J. Phys. D: Appl. Phys.* **37** 3088

[68] Wedding A B, Blevin H A and Fletcher J 1985 *J. Phys. D: Appl. Phys.* **18** 2361

[69] Roznerski W 1996 *J. Phys. D: Appl. Phys.* **29** 614

[70] Snelson R A and Lucas J 1975 Laplace Database, http://lxcat.net/LAPLACE, (Accessed: 03 January, 2018)

[71] Kelly L J 1990 *PhD Thesis* Flinders University of South Australia

[72] Campbell L, Brunger M J, Nolan A M, Kelly L J, Wedding A B, Harrison J, Teubner P J O, Cartwright D C and McLaughlin B 2001 *J. Phys. B: At. Mol. Opt. Phys.* **34** 1185

[73] White R D, Robson R E, Morrison M A, Li B and Ness K F 2007 *J. Phys.: Conf. Ser.* **71** 012004

[74] Janssen J F J, Pitchford L C, Hagelaar G J M and van Dijk J 2016 *Plasma Sources Sci. Technol.* **25** 055026

[75] Robson R E 1991 *Aust. J. Phys.* **44** 685

[76] White R D, Casey M J E, Stokes P, Bošnjaković D, Simonivic I, Brunger M J, de Urquijo J, Dujko S, Petrović Z Lj and Robson R E *Plasma Sources Sci. Technol.* in preparation